10.2514/6.2023-4205

Injection Duct Height Distribution Control for Co-Flow Jet Airfoil

Yan Ren * Gecheng Zha †
Coflow Jet, LLC.
PO Box 248662, Coral Gables
FL 33124, USA

Abstract

This paper presents the design of injection duct with height distribution control for co-flow jet (CFJ) flow control airfoils in cruise condition. The duct cross section outlines are mathematically modeled as superellipse with a duct height control parameter $c(Z, L)$. The injection duct height distribution is of great importance to the overall performance of the duct and the CFJ airfoil. The aerodynamic performance of the ducts and the CFJ airfoils are evaluated via numerical simulations, which employ 3D RANS solver with Spalart-Allmaras (S-A) turbulence model, 3th order WENO scheme for the inviscid fluxes, and 2nd order central differencing for the viscous terms. The design goal is to eliminate flow separation at the CFJ airfoil edges, maximize the corrected aerodynamic efficiency $(C_L/C_D)c$ of the CFJ airfoil. Results show that the injection duct height distribution control effectively removes flow separation at the airfoil edges. The best design presents 39% improvement of C_L/C_D and 16.4% improvement of $(C_L/C_D)c$.

Nomenclature

SD	Suction duct
ID	Injection duct
AFC	Active Flow Control
CFJ	Co-Flow Jet
LE	Leading edge
TE	Trailing edge
$FASIP$	Flow-Acoustics-Structure Interaction Package
$RANS$	Reynolds-Averaged Navier-Stokes
$ZNMF$	Zero-Net Mass Flux
η	Superellipse shape parameter
β	Deviation angle
P_{tr}	Total pressure recovery
M	Mach number
Γ	Gamma function
ρ	Density
V	Velocity
P_{01}	Total pressure at the inlet

* Coflow Jet, LLC., Chief Technology Officer, Ph.D., AIAA member
† Coflow Jet, LLC., President, AIAA Associate Fellow, Professor of the University of Miami

P_{02}	Total pressure at the outlet
$\dot{m}$	Mass flow rate
$_\infty$	Subscript, stands for free stream
$_{cs}$	Subscript, stands for cross section
$_i$	Subscript, stands for inlet
$_o$	Subscript, stands for outlet

1 Introduction

In the past three decades, Active Flow Control (AFC) has attracted lots of interests as a means to enhance the performance of airfoil, which otherwise has appeared to be saturated based on conventional airfoil shape optimization. Co-Flow Jet (CFJ) airfoil is a zero-net mass-flux (ZNMF) flow control method recently developed by Zha et al. [1, 2, 3, 4, 5, 6, 7, 8, 9, 10, 11]. It is demonstrated to achieve radical lift augmentation, stall margin increase, drag reduction and moderate nose-down moment for stationary and pitching airfoils.

In the CFJ airfoil concept, an injection slot near the leading edge (LE) and a suction slot near the trailing edge (TE) on the airfoil suction surface are created. As shown in Fig. 1, a small amount of mass flow is withdrawn into the suction duct, pressurized and energized by a micro-compressor, and then injected near the LE tangentially to the main flow via an injection duct. The whole process does not add any mass flow to the system and hence is a ZNMF flow control. The flow inside the airfoil (in the suction and injection ducts) are essential to the overall CFJ airfoil performance. Any flow separations within the ducts will increase the energy expenditure. The injection duct is more challenging to design than the suction duct because the flow existing from the compressor always has some swirl angle. The flow at the injection duct is prone to flow separation and the jet tends to have spanwise velocity, which is not desirable for the flow control. The purpose of this paper is to introduce injection duct height distribution control to resolve the above problem and achieve more favorable flow property distribution along the span at the duct outlet.

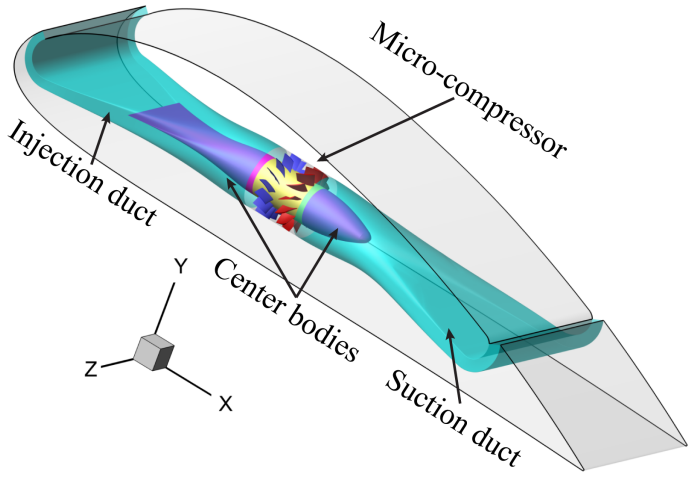

Figure 1: Schematic plot of a typical CFJ airfoil.

2 Methodology

2.1 Duct Geometry

As shown in Fig. 1, the duct inlet and outlet have different shapes. The inlet of suction duct and outlet of injection duct have rectangular shape, whereas the outlet of suction duct and inlet of injection duct have circular shape. The method of calculating circular-to-rectangular transition surfaces developed in [12] is adopted.

A circle, an ellipse, and a rectangle are all specific cases of superellipses. The locus of points which make up a superellipse is defined as:

$$(\frac{y}{a})^{\eta} + (\frac{z}{b})^{\eta} = 1 \tag{1}$$

where a and b are semi major and minor axis of the superellipse. η is shape parameter which controls the superellipse shape. The area enclosed by the superellipse A_{cs} can be computed as follows [13]:

$$A_{cs} = \frac{\Gamma(1/\eta)^2 4ab}{(\Gamma(2/\eta)2\eta)} \tag{2}$$

where Γ refers to the "gamma function" and is defined as:

$$\Gamma(\eta) = \int_0^{\infty} (e^{-t}t^{\eta-1})dt \quad (\eta > 0) \tag{3}$$

With A_{cs}, a and b defined as continuous analytic functions of x (axis distance from the entrance), the transition surface is determined by iteratively computing $\eta(x)$ from Eq. (4). For practical applications, a rectangle ($\eta = \infty$) is accurately approximated with $\eta \geq 50$. In this paper, $\eta = 100$ is used to represent a rectangle.

As shown in Fig. 2 (a), the CFJ airfoil injection and suction slot dimensions and locations are determined according to our previous published 2D design [14]. The injection and suction duct meanlines are determined based on the slot locations (blue curves in Fig. 2). We create superellipses along those duct meanlines, which pass through the superellipse geometric centers and locally perpendicular to the superellipses. The duct surfaces are formed by connecting those superellipses. Based on above mathematical model and geometry configuration, we successfully parameterize the problem, which is essential to the designs of the CFJ injection and suction ducts. In addition, the duct span over the diameter of the micro compressor outlet (W/D, Fig. 2 b) is fixed as 6 in this paper, which is pretty high and challenging to achieve high aerodynamic efficiency. High W/D results in fast flow expansion in duct span wise direction, which lead to non-uniform flow property distribution at the injection duct outlet. Duct height control is needed to achieve more favorable jet profile at the duct outlet.

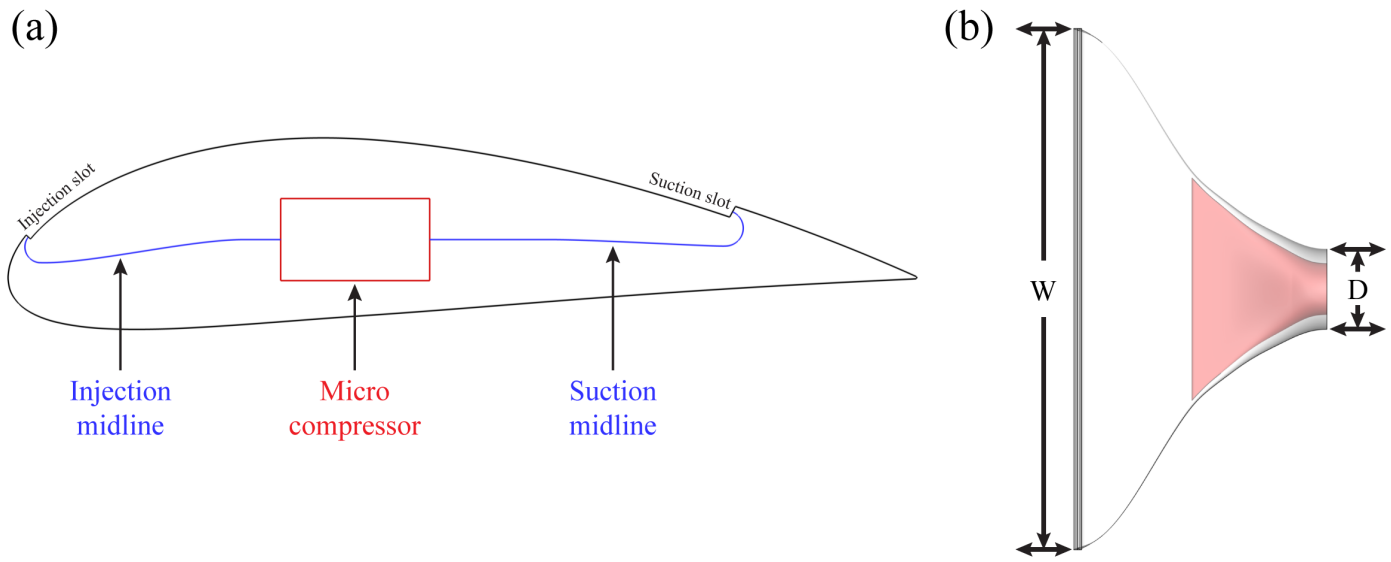

Figure 2: (a) CFJ airfoil configuration in cruise condition; (b) Definition of the duct W and D. The airfoil used here is CFJ-NACA 6421.

The duct height distribution control is defined as:

$$T_2(Z, L) = T_1(Z, L) \cdot c(Z, L) \tag{4}$$

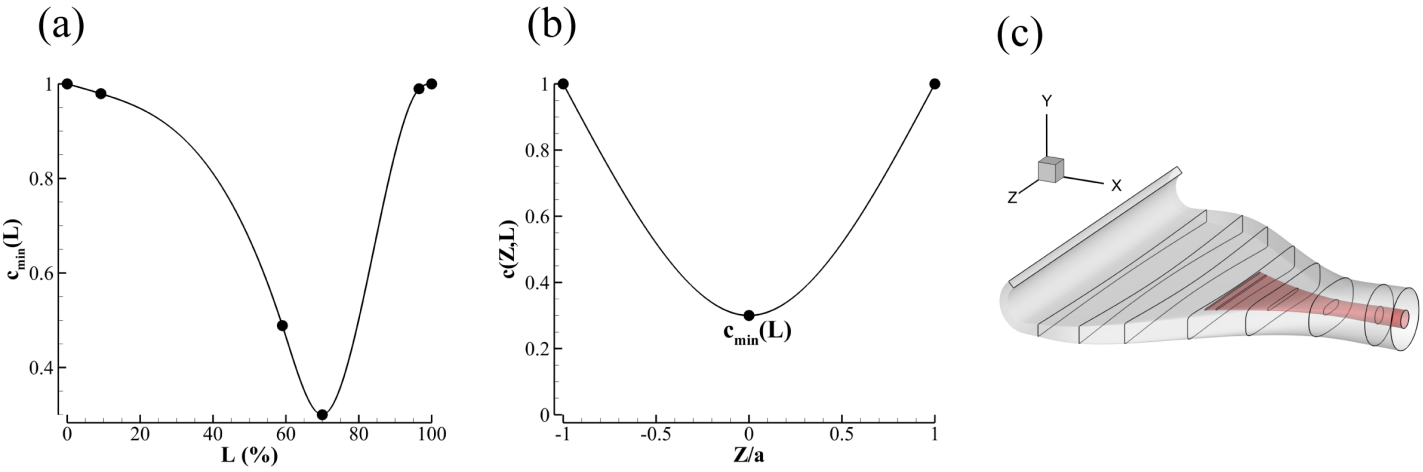

Figure 3: Schematic plots of (a) user specified c_{min} distribution along the injection duct; (b) c distribution in span wise direction of a specific duct cross section, which is a spline curve with sample points $(0, 1)$, $(0, c_{min})$, and $(1, 1)$; (c) a injection duct with height control.

where T_2 is the duct height distribution after height control, T_1 is the duct height distribution of a specific duct cross section (superellipse) before height control, c is the height correction parameter, Z and L are the coordinates in duct span wise direction and stream wise direction, respectively. To control the height of a duct, the user should first specify the $c_{min}(L)$ distribution along the duct (Fig. 3 a). Then the duct height distribution parameter $c(Z, L)$

along the duct span will be determined via a three points spline curve with sample points $(0, 1)$, $(0, c_{min})$, and $(1, 1)$. Fig. 3 (c) shows a typical injection duct with height control.

2.2 CFD Simulation Setup

The FASIP (Flow-Acoustics-Structure Interaction Package) CFD code is used to conduct the numerical simulation. The 3D Reynolds Averaged Navier-Stokes (RANS) equations with one-equation Spalart-Allmaras [15] turbulence model is used. A 3rd order WENO scheme for the inviscid flux [16, 17, 18, 19, 20, 21] and a 2nd order central differencing for the viscous terms [16, 20] are employed to discretize the Navier-Stokes equations. The low diffusion E-CUSP scheme used as the approximate Riemann solver suggested by Zha et al [17] is utilized with the WENO scheme to evaluate the inviscid fluxes. Implicit time marching method using Gauss-Seidel line relaxation is used to achieve a fast convergence rate [22]. Parallel computing is implemented to save wall clock simulation time [23].

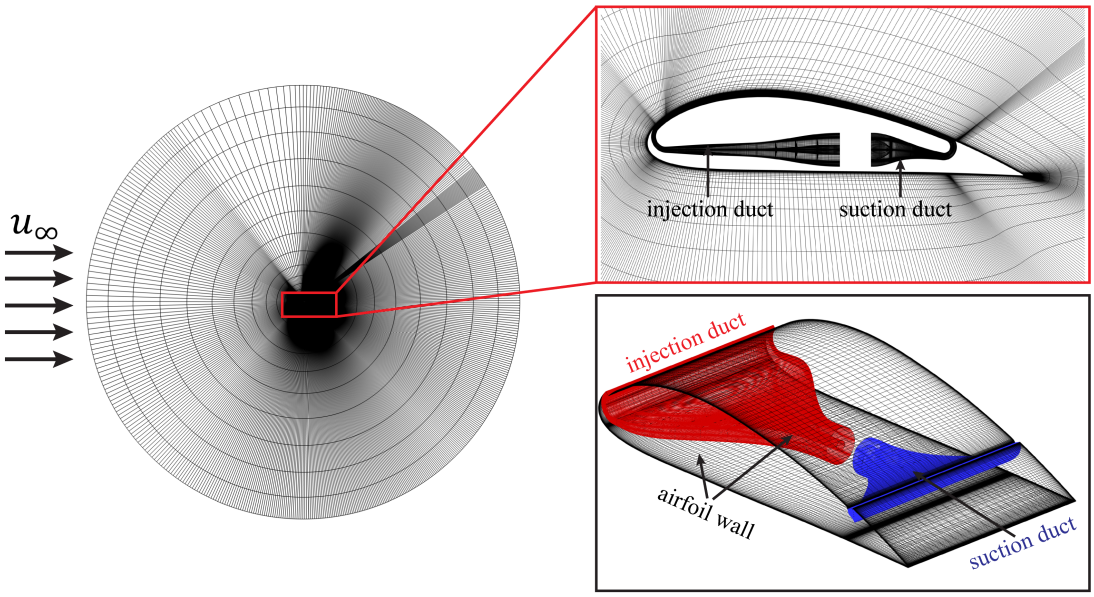

Figure 4: Computational mesh used in the current study.

The 3rd order accuracy no slip condition is enforced on the solid surface with the wall treatment suggested in [24] to achieve the flux conservation on the wall. The computational mesh is shown in Fig. **??**. Total pressure, total temperature and flow angles are specified at the injection duct inlet, as well as the upstream portion of the far field. Constant static pressure is applied at the suction duct outlet as well as the downstream portion of the far field. The micro-compressor inlet and outlet profiles[25] are used as the boundary conditions of the suction duct outlet and injection inlet to simulate the micro-compressor actuator effects. Symmetry boundary conditions are applied at the two sides in z-direction to ensure the effect of a segment of a 3D CFJ wing. The cross-section faces of the ducts are meshed using "H" topology while the parts around the airfoil are meshed using "O" topology. The total mesh size is 11.376 millions points, split into 192 blocks for the parallel computation. The first grid point on the wing surface is placed at $y^+ \approx 1$.

3 Results

Four different designs of the injection duct, a baseline case without duct height control and three designs (D1, D2, and D3) with duct height control, are discussed in this section. Fig. 5 (a) and (b) show the injection duct geometry of the baseline case. A center body (red colored) is located inside the injection duct to guide the flow to prevent flow separation. The $W/D = 6$ for all cases discussed in this paper. Fig. 5 (c) shows the c_{min} distribution used to control the duct height for the case D1, D2, and D3. Fig. 5 (d) shows the cross sectional area distribution along the ducts of the four cases. The jet momentum coefficient $C_\mu = 0.03$ for all cases discussed in this paper.

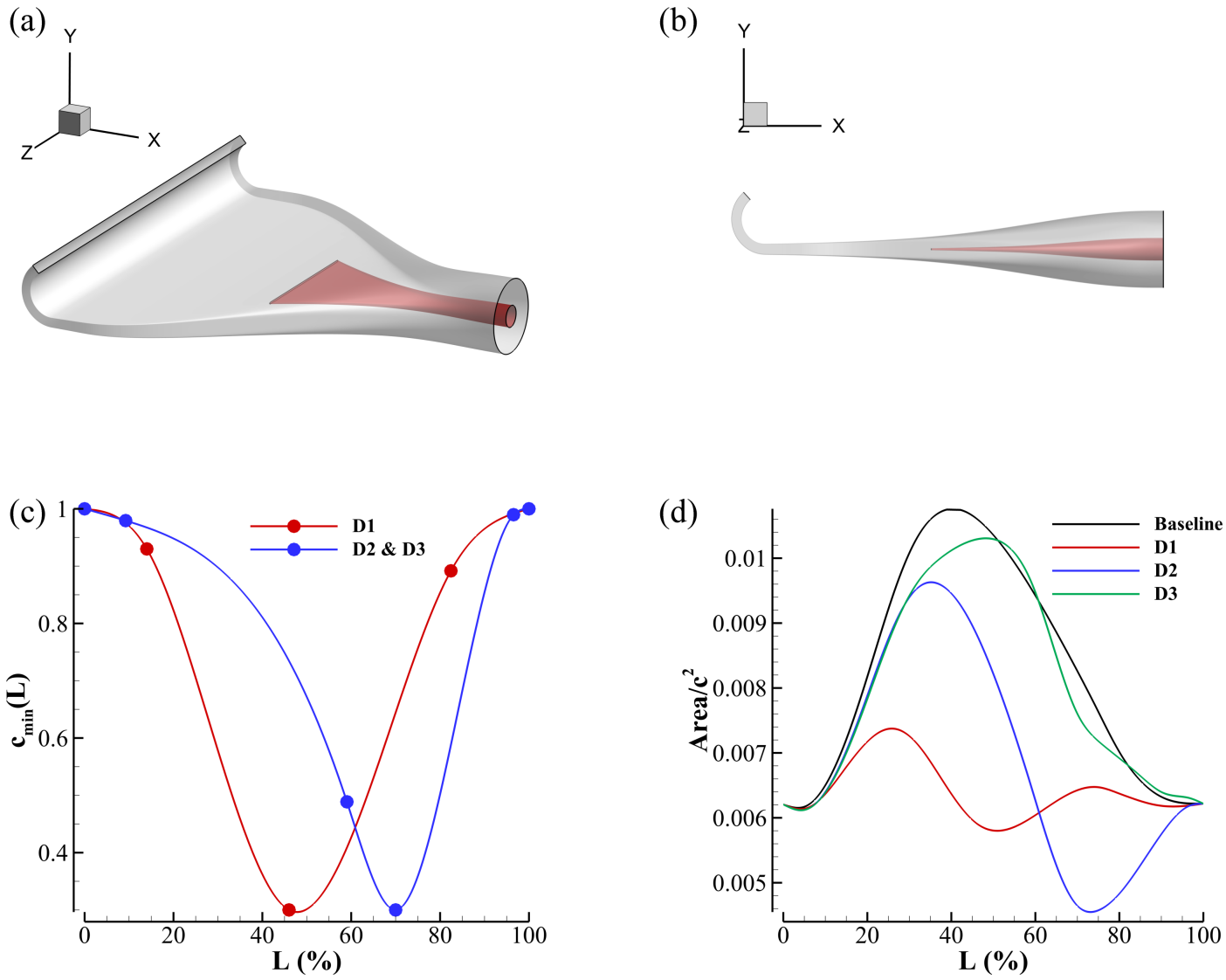

Figure 5: (a) perspective view of the baseline injection duct; (b) side view of the baseline injection duct; (c) c_{min} distribution of D1, D2, and D3; (d) cross sectional area distribution along the ducts of baseline, D1, D2, and D3.

Table 1 lists the aerodynamic performance of the four cases. We can see that the cases with height control show higher C_L and lower C_D. The best C_L/C_D is 83.91 for the case D3, which is 39% improvement comparing to the baseline case. However, the total pressure recovery of the case D1 and D2 dropped a lot, and it leads to higher

power consumption of the compressor. The corrected aerodynamic efficiency $(C_L/C_D)_c$ decreased a little bit for the case D1 and D2. The height control of the injection duct affects the duct cross sectional area distribution, and results in the decrease of the total pressure recovery. Case D3 presents the same height control as the case D2, but with much favorable cross sectional area distribution, which is similar to the baseline case. The total pressure recovery improved a lot for the case D3, and the power consumption of the compressor decreased. The corrected aerodynamic efficiency $(C_L/C_D)_c = 42.81$ for the case D3, which shows 16.4% improvement comparing to the baseline case.

Table 1: Aerodynamic performance of the current designs.

Cases	C_μ	C_L	C_D	P_C	C_L/C_D	$(C_L/C_D)_c$	P_{tr}
Baseline	0.03	1.215	0.0201	0.0129	60.39	36.77	98.2%
D1	0.03	1.263	0.0176	0.0187	71.76	34.84	96.5%
D2	0.03	1.290	0.0155	0.0213	83.29	35.03	96.1%
D3	0.03	1.290	0.0154	0.0148	83.91	42.81	98.1%

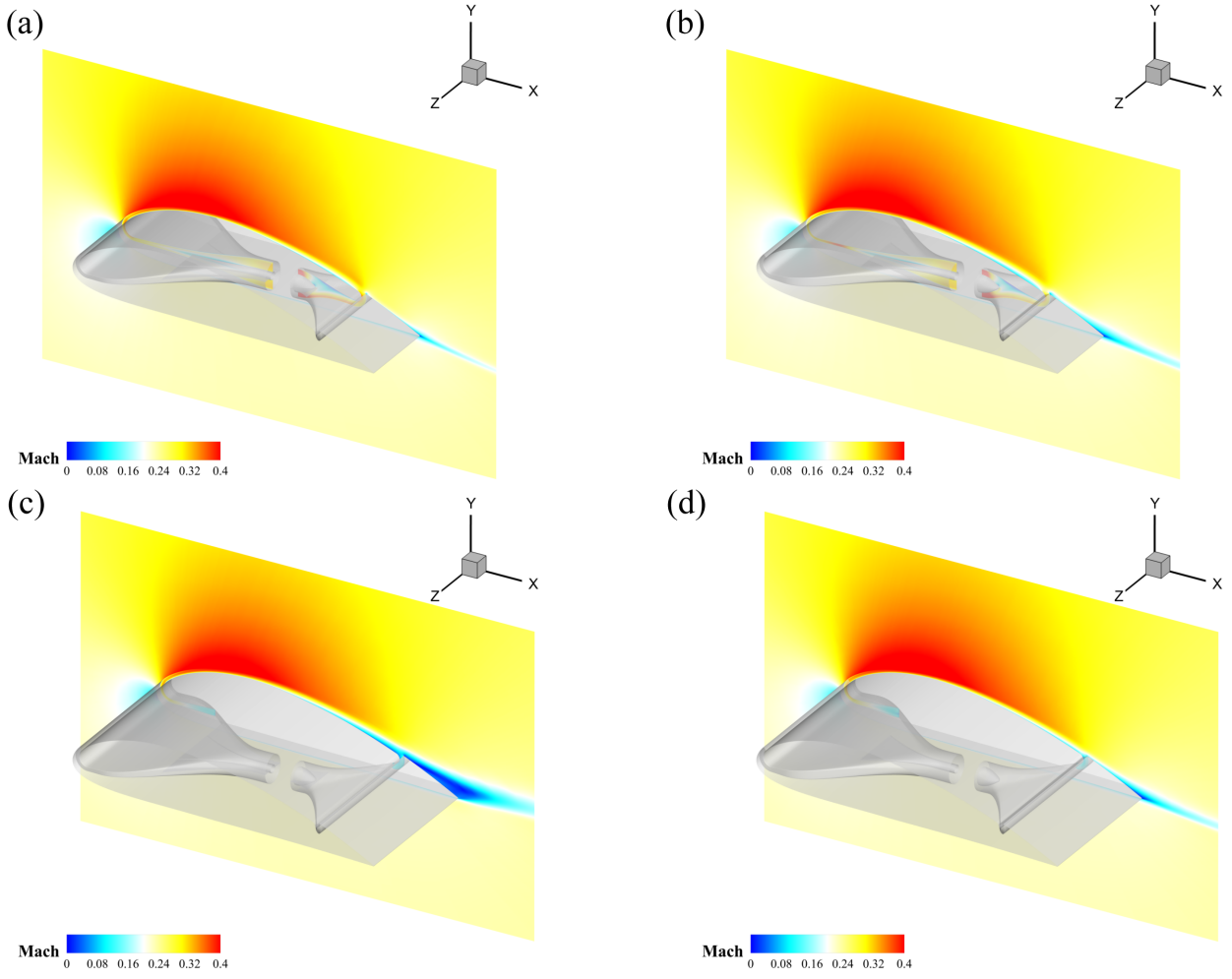

Figure 6: (a) mid chord flow slice of the baseline design; (b) mid chord flow slice of the case D3; (c) edge slice of the baseline design; (d) edge slice of the case D3.

Fig. 6 shows the flow slices at the mid chord and edge of the CFJ airfoils. The baseline case and the best efficiency case D3 are discussed here. As shown in Fig. 6 (a) and (b), no flow separation can be observed for both cases. The flow attaches well at the mid chord for both cases. For the airfoil edge flow slices, the baseline case presents large flow separation at the trailing edge suction surface of the airfoil, while no significant flow separation can be observed for the case D3. The injection duct height control successfully push more flow to the airfoil edges, enhances flow control at the airfoil edge and prevent flow separation.

Fig. 7 shows the 3D streamlines inside the injection duct and flow slice at the duct mean line for the baseline case and the case D3. The streamlines and flow slices are colored by Mach number. A high speed zone can be identified downstream of the duct center body for the case D3, where exactly the minimum duct height happens due to the duct height control. Such height control pushes more flow to the sides and enhances jet velocity at the two edges of the duct outlet.

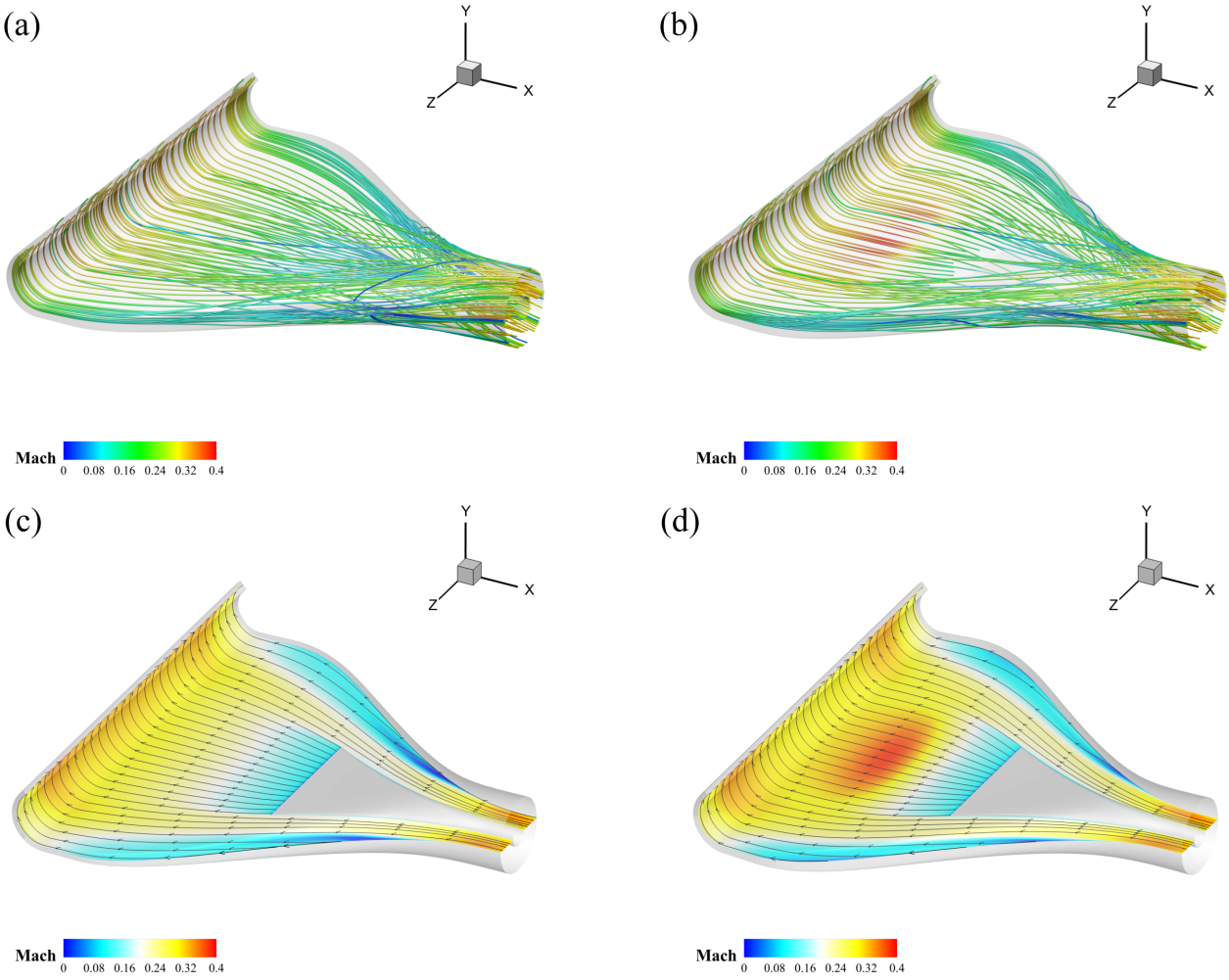

Figure 7: (a) streamlines inside the injection duct for the baseline case; (b) streamlines inside the injection duct for the case D3; (c) flow slice at the duct mean line for the baseline case; (d) flow slice at the duct mean line for the case D3.

Fig. 8 (a) and (b) show the stream wise and span wise jet velocity along the duct span at the injection duct outlet for all four cases. We can see that the cases with height control present much higher stream wise velocity at

the edges, and lower stream wise velocity at the middle part. For the span wise jet velocity, it is worth noting that the profile phase reversed for the case D2 and D3 comparing to the baseline case. The jet direction at the edge is more pointing towards the duct center due to the height control. Fig. 8 (c) shows the total pressure distribution along the duct for all cases. It is clear to see that the baseline case and the case D3 present much better total pressure recovery due to a fine tuned cross sectional area design.

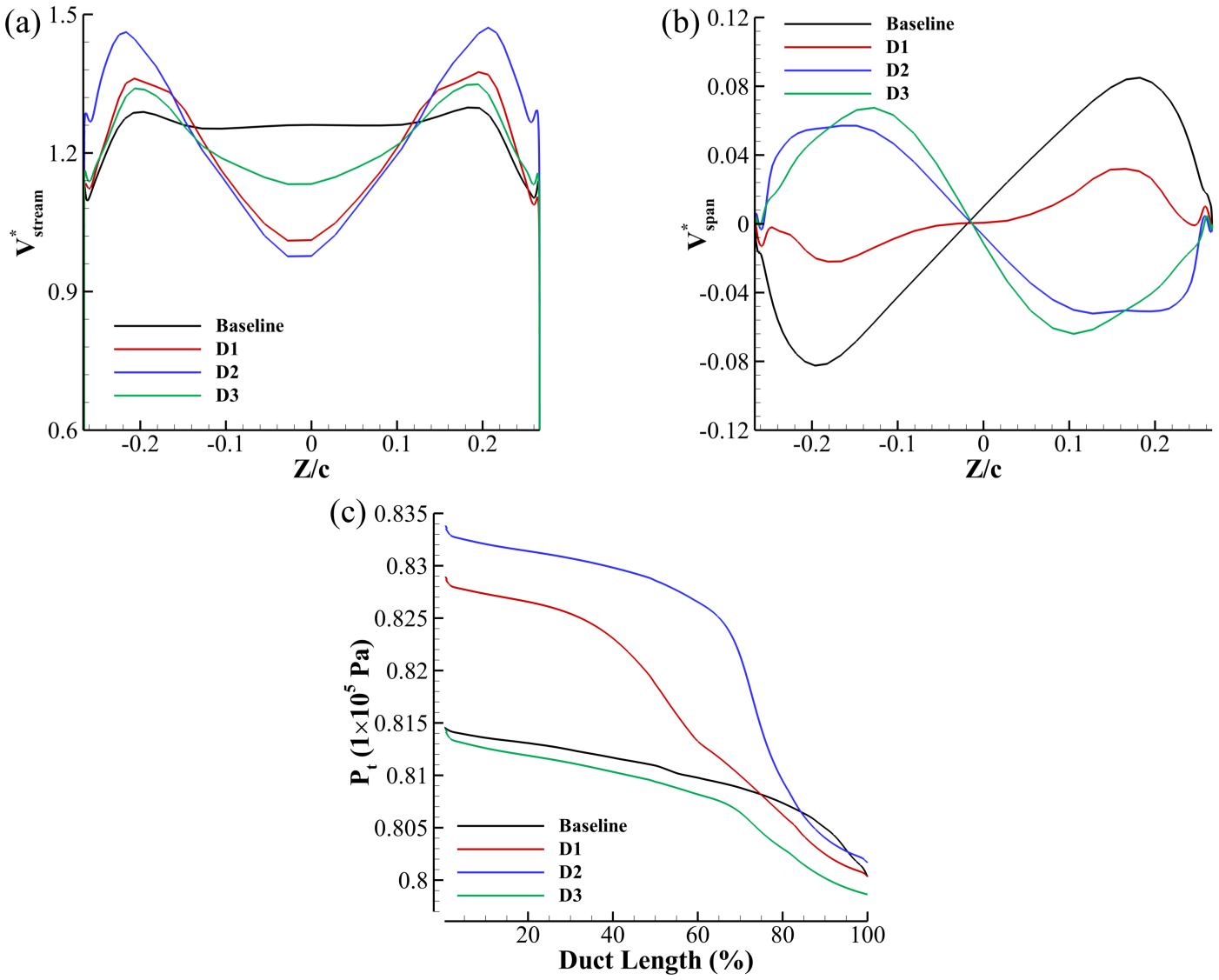

Figure 8: (a) stream wise velocity distribution along the duct span at the duct outlet; (b) span wise velocity distribution along the duct span at the duct outlet; (c) total pressure distribution along the ducts.

4 Conclusion

This paper presents the design of injection duct with height distribution control for co-flow jet (CFJ) flow control airfoils in cruise condition. Four different designs of the injection duct, a baseline case without duct height control and three designs with duct height control, are discussed in this study. Results show that the injection

duct with the minimum duct height (50% of the baseline) at 70% duct span presents the best performance. Also, a diverging-converging cross-sectional area distribution of the injection duct is more faverable. The injection duct height distribution control effectively removes flow separation at the airfoil edges. The best design presents 39% improvement of C_L/C_D and 16.4% improvement of $(C_L/C_D)c$.

References

[1] G.-C. Zha and D. C. Paxton, "A Novel Flow Control Method for Airfoil Performance Enhancement Using Co-Flow Jet." *Applications of Circulation Control Technologies*, Chapter 10, p. 293-314, Vol. 214, Progress in Astronautics and Aeronautics, AIAA Book Series, Editors: Joslin, R. D. and Jones, G.S., 2006.

[2] G.-C. Zha, W. Gao, and C. Paxton, "Jet Effects on Co-Flow Jet Airfoil Performance," *AIAA Journal, No. 6,*, vol. 45, pp. 1222–1231, 2007.

[3] G.-C. Zha, C. Paxton, A. Conley, A. Wells, and B. Carroll, "Effect of Injection Slot Size on High Performance Co-Flow Jet Airfoil," *AIAA Journal of Aircraft*, vol. 43, 2006.

[4] G.-C. Zha, B. Carroll, C. Paxton, A. Conley, and A. Wells, "High Performance Airfoil with Co-Flow Jet Flow Control," *AIAA Journal*, vol. 45, 2007.

[5] Wang, B.-Y. and Haddoukessouni, B. and Levy, J. and Zha, G.-C., "Numerical Investigations of Injection Slot Size Effect on the Performance of Co-Flow Jet Airfoil," *Journal of Aircraft*, vol. Vol. 45, No. 6,, pp. pp.2084–2091, 2008.

[6] B. P. E. Dano, D. Kirk, and G.-C. Zha, "Experimental Investigation of Jet Mixing Mechanism of Co- Flow Jet Airfoil." AIAA-2010-4421, 5th AIAA Flow Control Conference, Chicago, IL, 28 Jun - 1 Jul 2010.

[7] B. P. E. Dano, G.-C. Zha, and M. Castillo, "Experimental Study of Co-Flow Jet Airfoil Performance Enhancement Using Micro Discreet Jets." AIAA Paper 2011-0941, 49th AIAA Aerospace Sciences Meeting, Orlando, FL, 4-7 January 2011.

[8] A. Lefebvre, B. Dano, W. Bartow, M. Fronzo, and G. Zha, "Performance and energy expenditure of coflow jet airfoil with variation of mach number," *Journal of Aircraft*, vol. 53, no. 6, pp. 1757–1767, 2016.

[9] A. Lefebvre, G-C. Zha, "Numerical Simulation of Pitching Airfoil Performance Enhancement Using Co-Flow Jet Flow Control," *AIAA paper 2013-2517*, June 2013.

[10] A. Lefebvre, G-C. Zha, "Cow-Flow Jet Airfoil Trade Study Part I : Energy Consumption and Aerodynamic Performance," *32nd AIAA Applied Aerodynamics Conference, AIAA AVIATION Forum, AIAA 2014-2682*, June 2014.

[11] A. Lefebvre, G-C. Zha, "Cow-Flow Jet Airfoil Trade Study Part II : Moment and Drag," *32nd AIAA Applied Aerodynamics Conference, AIAA AVIATION Forum, AIAA 2014-2683*, June 2014.

[12] J. R. Burley II, L. S. Bangert, and J. R. Carlson, "Static investigation of circular-to-rectangular transition ducts for high-aspect-ratio nonaxisymmetric nozzles." NASA Technical Paper 2534, 1986.

[13] W. H. Beyer, "Crc standard mathematical tables," *West Palm Beach, Fl.: Chemical Rubber Co., 1978, 25th ed., edited by Beyer, William H.*, 1978.

[14] Yang, Yunchao and Zha, Gecheng, "Super-Lift Coefficient of Active Flow Control Airfoil: What is the Limit?," *AIAA Paper 2017-1693, AIAA SCITECH2017, 55th AIAA Aerospace Science Meeting, Grapevine, Texas*, p. 1693, 9-13 January 2017.

[15] P. R. Spalart and S. R. Allmaras, "A one-equation turbulence model for aerodynamic flows," in *30th Aerospace Sciences Meeting and Exhibit, Aerospace Sciences Meetings, Reno, NV, USA, AIAA Paper 92-0439*, 1992.

[16] Y.-Q. Shen and G.-C. Zha, "Large Eddy Simulation Using a New Set of Sixth Order Schemes for Compressible Viscous Terms ," *Journal of Computational Physics*, vol. 229, pp. 8296–8312, 2010.

[17] Zha, G.C., Shen, Y.Q. and Wang, B.Y., "An improved low diffusion E-CUSP upwind scheme ," *Journal of Computer and Fluids*, vol. 48, pp. 214–220, Sep. 2011.

[18] Y.-Q. Shen and G.-Z. Zha , "Generalized finite compact difference scheme for shock/complex flowfield interaction," *Journal of Computational Physics*, vol. doi:10.1016/j.jcp.2011.01.039, 2011.

[19] Shen, Y.-Q. and Zha, G.-C. and Wang, B.-Y., " Improvement of Stability and Accuracy of Implicit WENO Scheme," *AIAA Journal*, vol. 47, No. 2, pp. 331–344, 2009.

[20] Shen, Y.-Q. and Zha, G.-C. and Chen, X.-Y., " High Order Conservative Differencing for Viscous Terms and the Application to Vortex-Induced Vibration Flows," *Journal of Computational Physics*, vol. 228(2), pp. 8283–8300, 2009.

[21] Shen, Y.-Q. and Zha, G.-C. , " Improvement of the WENO Scheme Smoothness Estimator," *International Journal for Numerical Methods in Fluids*, vol. DOI:10.1002/fld.2186, 2009.

[22] G.-C. Zha and E. Bilgen, "Numerical Study of Three-Dimensional Transonic Flows Using Unfactored Upwind-Relaxation Sweeping Algorithm," *Journal of Computational Physics*, vol. 125, pp. 425–433, 1996.

[23] B.-Y. Wang and G.-C. Zha, "A General Sub-Domain Boundary Mapping Procedure For Structured Grid CFD Parallel Computation," *AIAA Journal of Aerospace Computing, Information, and Communication*, vol. 5, No.11, pp. 2084–2091, 2008.

[24] Y.-Q. Shen, G.-C. Zha, and B.-Y. Wang, "Improvement of Stability and Accuracy of Implicit WENO Scheme ," *AIAA Journal*, vol. 47, pp. 331–344, 2009.

[25] PCA engineers, "Design of a mixed flow fan." Internal Report to University of Miami, 2017.